Potential for nocturnal satellite detection of suspended matter concentrations in coastal waters using a panchromatic band: a feasibility study based on VIIRS (NASA/NOAA) spectral and radiometric specifications

Malik Chami, Morgane Larnicol, Sébastien Migeon, Audrey Minghelli, Sandrine Mathieu

Research Article | Vol. 28, No. 10 / 11 May 2020 / Optics Express 15314
Optics EXPRESS

Potential for nocturnal satellite detection of suspended matter concentrations in coastal waters using a panchromatic band: a feasibility study based on VIIRS (NASA/NOAA) spectral and radiometric specifications

MALIK CHAMI,[1,2,*] MORGANE LARNICOL,[3] SEBASTIEN MIGEON,[4,5] AUDREY MINGHELLI,[6] AND SANDRINE MATHIEU[7]

[1] *Sorbonne Université, CNRS-INSU, Laboratoire Atmosphères Milieux Observations Spatiales (LATMOS), Boulevard de l'Observatoire, CS 34229, 06304 Nice Cedex, France*
[2] *Institut Universitaire de France, Ministère de l'Education Nationale, de l'Enseignement Supérieur et de la Recherche, 1 rue Descartes, 75231 Paris Cedex 05, France*
[3] *Observatoire Côte d'Azur, CNRS, Laboratoire Lagrange, Boulevard de l'Observatoire, CS 34229, 06304 Nice Cedex, France*
[4] *Université Côte d'Azur, CNRS, OCA, IRD, Géoazur (UMR 7329), 250 rue A. Einstein, 06560 Valbonne, France*
[5] *Sorbonne Université, UFR939, 06230 Villefranche-sur-Mer, France*
[6] *Université de Toulon, CNRS, SeaTech, Laboratoire LIS, UMR 7020, 83041 Toulon, France*
[7] *Thales Alenia Space, 5 allée des Gabians, 06156 Cannes la Bocca Cedex, 06150 Cannes, France*
[*] *malik.chami@upmc.fr*

Abstract: Satellite remote sensing of coastal waters is important for understanding the functioning of these complex ecosystems. High satellite revisit frequency is required to permit a relevant monitoring of the strong dynamical processes involved in such areas, for example rivers discharge or tidal currents. One key parameter that is derived from satellite data is the suspended particulate matter (SPM) concentration. Knowledge of the variability of SPM could be used by sediment transport models for providing accurate predictions. Most of the current satellites that are dedicated to ocean color observations have a sun-synchronous orbit that performs a single daytime observation. The Visible Infrared Imaging Radiometer Suite (VIIRS) ocean color sensor (NASA/NOAA) is the only one that is equipped with a panchromatic spectral band, so-called Day-Night Band, which is able to measure extremely low level signals, typically of the order of magnitude of 10^{-5} W m^{-2} sr^{-1}µm^{-1}. The objective of this paper is to investigate the potential of the panchromatic and radiometric specifications of the VIIRS sensor to detect SPM concentrations from nighttime satellite observations. Realistic radiative transfer simulations are performed to quantitatively determine the amplitude of the top of atmosphere radiances under various conditions such as various moon incident illuminations, observation geometries, atmospheric and oceanic turbidities. The simulations are compared with the minimum detectable radiance as specified for the VIIRS sensor. The results show that the detection of SPM is systematically feasible, including in clear waters, for any observation geometries in the case of a full moon illumination. The sensitivity of the results to the lunar phase (i.e., out of the full moon conditions), which is one of the originalities of the study, shows that the detection should also be feasible for a significant number of nights over the entire lunar cycle, typically from 5 to 15 nights depending on the water turbidity. Therefore, nighttime ocean color panchromatic measurements performed using a VIIRS-like sensor are a highly promising approach, especially if it is combined with daytime observations, for improving the monitoring of ocean dynamics.

#393048 https://doi.org/10.1364/OE.393048
Journal © 2020 Received 18 Mar 2020; revised 28 Apr 2020; accepted 28 Apr 2020; published 5 May 2020

Optics EXPRESS

1. Introduction

Satellite remote sensing of the ocean color is of great interest to provide insight into global ocean variability in the context of climate processes and ecosystem health. Examples of the parameters that can be derived from ocean color data are typically the chlorophyll-a pigment concentration (Chl-a), which is informative on the phytoplankton biomass, and the suspended particulate matter concentration, hereafter referred to as SPM. The estimation of SPM concentrations from satellite measurements is important to gain understanding of the functioning of coastal ecosystems such as the exchange of matter between land and ocean, the river sediment discharge into the ocean, the water quality, the underwater vision, and the primary production estimates. Therefore, the SPM parameter and its relation to marine resources are important factors economically, especially for littoral countries. The past, present and forthcoming ocean color satellite sensors such as Sea-viewing Wide Field-of-View Sensor (SeaWiFS) (NASA) [1], Moderate Resolution Imaging Spectroradiometer (MODIS) (NASA) [2], Copernicus Sentinel 3/Ocean and Land Color Instrument (OLCI) (Copernicus/ESA) [3], and Plankton Aerosol Cloud ocean Ecosystem (PACE)/Ocean Color Instrument (OCI) (NASA) [4], are designed to perform daytime measurements of the reflected sunlight at various spectral bands. This is because the satellites that carry these sensors are characterized by a sun-synchronous orbit which allows data to be acquired at the same local time, typically around mid-day, for a given site. Thus, it is not such a great challenge to define and to build the spectral radiometric specifications required for deriving the ocean color parameters due to the sufficient amount of sunlight illuminating the scene. As an example, the minimum top of atmosphere radiance that could be measured at 560 nm by the current Copernicus Sentinel 3/OLCI sensor is 12.7 W m^{-2} μm^{-1} sr^{-1} [3]. Note that the value of the top of atmosphere radiance that has been recently proposed by the scientific ocean color community for designing the future generation of ocean color sensors is about three times higher, namely 33.9 W m^{-2} μm^{-1} sr^{-1}, at the same wavelength [5]. Single sun-synchronous daytime measurements performed by the ocean color sensors limit our ability to fully characterize and monitor rapid processes or events occurring in coastal zones, such as the fast variation of SPM concentrations induced by river runoff, which could significantly vary with time over the course of the day and at night due to the strong ocean dynamics.

The Visible Infrared Imaging Radiometer Suite (VIIRS) satellite ocean color sensor on the Suomi National Polar-orbiting Partnership (SNPP) (2011–present) and on NOAA-20 (2017–present) [6] is equipped with an original Day-Night Band (DNB) which provides a unique ability to measure extremely low-levels of visible/near-infrared light, typically in the range [400 nm – 900 nm]. The minimum top of atmosphere radiance that could be measured by VIIRS for such DNB is 3.10^{-5} W m^{-2} μm^{-1} sr^{-1} [7]. The DNB thus allows the measurement of signal about 1 million times lower than the signals typically measured by conventional spectral bands used by the current daytime ocean color sensors such as the Copernicus Sentinel 3/OLCI sensor above mentioned. Therefore, the VIIRS sensor offers the relevant capability of performing nocturnal measurements of the radiance exiting the ocean. Miller et al. [8] carried out a valuable review study that illustrates the high potential of using night measurements acquired in the DNB of the VIIRS sensor to broaden knowledge on a great variety of research fields such as the cryosphere, the atmosphere, the biosphere and the lithosphere. As reported by Miller et al. [8], VIIRS-like nighttime satellite measurements could be used, for example, to investigate the sea ice edge, the sea surface roughness properties, the soil moisture, biomass burning, city lights, the evolution of high turbidity features, and even marine bioluminescence. More recently, Shi and Wang [9] illustrated the potential of the VIIRS DNB for nocturnal observation ocean dynamics such as the sediment front movement, the phytoplankton bloom migration, and the complex estuary dynamics at night. As highlighted by Miller et al. [8] and by Shi and Wang [9], more studies are still required to explore in depth capability of exploiting night low-light visible measurements for improving knowledge on all of the research domains mentioned above. This

Optics EXPRESS

paper aims to take another step forward in investigating the potential of nighttime ocean color data for the monitoring of turbidity in coastal waters.

The objectives of this study are (i) to carefully examine whether the top of atmosphere radiance induced by various SPM concentrations in coastal waters is measurable at night based on VIIRS radiometric specifications (minimum radiance), (ii) to investigate whether the SPM concentrations could possibly be quantified at night depending on the turbidity, and (iii) to provide the potential number of nights over the course of one lunar cycle for which the detection and quantification of SPM concentrations would be feasible. It should be highlighted that this study goes one step beyond Shi and Wang's study [9] inasmuch as their study showed the feasibility of observing SPM at night in turbid waters while the current study relies on a more quantitative analysis of the radiometric minimum requirements for expanding the use of observations of the water turbidity from daytime to nighttime light conditions. To reach these objectives, radiative transfer modelling is used to simulate the top of atmosphere radiances under various lunar illuminations. The values and the ranges of variation of the radiative transfer model inputs are determined as far as possible from in-situ bio-optical datasets acquired in coastal areas, thus providing us with simulations close to real-world marine conditions. A benchmark case of simulation is first analyzed prior to performing a sensitivity study of the results over various configurations that are representative of satellite observations (e.g., atmospheric and oceanic turbidities, observation geometries). The paper is organized as follows: the data used for this study as inputs of the radiative transfer model, namely the lunar irradiance features and the bio-optical oceanic datasets, and the radiative transfer modelling aspects are described in Section 2. The quantitative results dealing with the expected values of the top of atmosphere radiances for the benchmark case and for a full moon illumination are presented in Section 3. The sensitivity of these results to various parameters such as the atmospheric and oceanic optical properties, and the observation geometry are also shown in Section 3. The influence of the amplitude of the moonlight illumination over the lunar cycle on the detection of SPM is discussed in Section 4.

2. Data and method

The methodology used to reach the objectives of the paper relies on the analysis of radiative transfer simulations at night. It is thus important to first characterize the moonlight illumination of the earth.

2.1. Lunar extraterrestrial irradiance

Knowledge of the lunar extraterrestrial irradiance, referred to as EL_{TOA} (in W m^{-2} μm^{-1}), is required to determine the geophysical values of the simulated top of atmosphere radiance (in W m^{-2} sr^{-1} μm^{-1}) that would be measured by a satellite sensor above the ocean at night. EL_{TOA} could be expressed as a function of the moon top of atmosphere radiance, referred to as LL_{TOA}, as follows [10] [Eq. (1)]:

$$EL_{TOA} = LL_{TOA} \times \Omega_{Lunar} \tag{1}$$

where Ω_{Lunar} is the solid angle (in sr) under which the moon is viewed from the earth; its value is 6.42 10^{-5} sr [10]; the values of the moon radiance LL_{TOA} were obtained from Stone et al. [11]. The maximum spectral value of EL_{TOA}, which is observed around 600 nm, is about 4 10^{-3} W m^{-2} μm^{-1}. As a comparison, the maximum spectral value of the solar extraterrestrial irradiance is around 2000 W m^{-2} μm^{-1} [12]. Therefore, the full moonlight illumination of the earth is about 1 million times lower than the sunlight illumination. Such a significant difference means that nighttime detection of the SPM in ocean waters necessarily requires a proper radiometric specification of a satellite sensor to measure low level signals, such as the DNB designed for the VIIRS sensor.

The lunar phase angle, referred to as φ_{Lunar}, is used to express the various phases of the moon over the course of the 29.5 nights lunar cycle (i.e. new moon, first quarter phase, full moon, last

Optics EXPRESS

quarter phase). The value of φ_{Lunar} linearly waxes from 180° (new moon) toward 0° (full moon) and then wanes back toward 180° (new moon), thus inducing a variable illuminated fraction of the moon [13]. However, it should be highlighted that the lunar brightness is characterized by a nonlinear behavior with the phase angle. Miller and Turner [13] proposed a model that accounts for such nonlinear feature to compute EL_{TOA}. Such a model, referred to as MT2009, has been used here to express EL_{TOA} as a function of φ_{Lunar} (Fig. 1). Two examples of the fractions of the lunar irradiance, referred to as F, are also shown in Fig. 1: $F_{100\%}$ is the notation used for the maximum lunar brightness (i.e., full moon, φ_{Lunar}=0°) and $F_{50\%}$ is the notation used for the half-maximum lunar brightness. Figure 1 clearly illustrates the non-linear relationship between the moonlight irradiance EL_{TOA} and the lunar phase angle. In particular, it is interesting to note that the value of the lunar phase angle for which the amplitude of moonlight illumination is half of that of the full moon illumination, $F_{50\%}$, is 28°, which is far lower than the phase angle corresponding to the half-moon condition (φ_{Lunar}=90°).

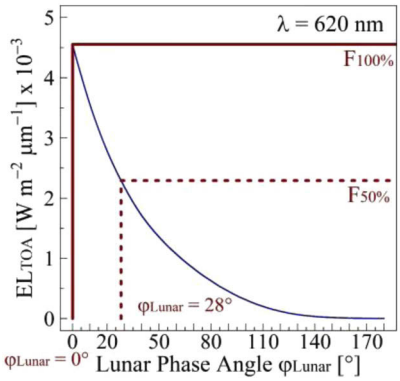

Fig. 1. Relationship between the top-of-atmosphere downwelling lunar irradiance EL_{TOA} (in W m^{-2} μm^{-1}) and the lunar phase angle φ_{Lunar} (in degrees) at 620 nm based on the Miller and Turner [13] model. The notation F is used to express the fraction of the lunar irradiance: $F_{100\%}$ means a full moon illumination (i.e., 100% of EL_{TOA}, φ_{Lunar}=0°) and $F_{50\%}$ means 50% of lunar brightness from the full moon (i.e., 50% of EL_{TOA}).

The lunar phase angle φ_{Lunar} could be used to express the total number of nights N_{nights} for which the moonlight illuminates the earth. Typically, the value of N_{nights} is 1 for the particular case of the full moon (φ_{Lunar}=0°) and 0 for the particular case of the new moon (φ_{Lunar}=180°). Out of the full moon and new moon conditions, the total number of nights N_{night} could be related to φ_{Lunar} using the symmetry property of the lunar phases on both sides of the full moon as follows [Eq. (2)]:

$$N_{nights} = [2 \times \varphi_{Lunar} \times 29.5 nights] / 360° \quad (2)$$

As a result from both Eq. (2) and the particular cases of the full moon and new moon phases, a table of correspondence between the total number of nights N_{nights} and the lunar phase angle φ_{Lunar} could be established (Table 1). Such a correspondence will be used later in the paper (Section 4). Note that the values corresponding to ± (N_{nights}/2) represent the number of nights on both sides of the full moon.

2.2. *In-situ bio-optical datasets*

Several inputs of the radiative transfer model are defined, based on in-situ bio-optical measurements acquired in different coastal zones around the world, to ensure the consistency of the simulated radiances with those observed in natural waters. In particular, the values of the Chl-a and SPM concentrations as well as the values of the colored dissolved organic matter (CDOM)

Optics EXPRESS

Table 1. Relationship between the lunar phase angle φ_{Lunar} and the total number of nights N_{nights} for which the earth is illuminated by moonlight. The notation $\pm\varphi_{Lunar}$ is used to account for the symmetry on both sides of the full moon (φ_{Lunar}=0°). The number of nights on both sides of the full moon, which is calculated as $\pm(N_{nights}/2)$, is also reported.

φ_{Lunar}	0° (Full Moon)	±30°	±60°	±90°	±120°	±150°	±180°
N_{nights}	1	4.9	9.8	14.8	19.7	24.6	0
$\pm(N_{nights}/2)$	-	±2.45	±4.9	±7.4	±9.85	±12.3	-

spectral absorption coefficient, hereafter referred to as a_{CDOM}, are determined using two well proven databases dedicated to ocean color applications, namely the SeaWiFS Bio-optical Archive and Storage System (SeaBASS) database [14] and the CoastColour Round Robin dataset (CCRR) [15]. Apart from the fact that they are publicly available, these datasets are highly relevant because they contain bio-optical measurements that have been collected at various sites at a global scale, including in coastal areas, thus making them eligible to account for the strong variability of the optical properties that could be found in coastal ecosystems. In addition, these datasets were primarily designed to be used for the validation of the satellite ocean color algorithms, thus meaning that they are composed of high quality controlled data.

The SeaBASS database has been developed by the NASA Ocean Biology Processing Group to archive biological, optical and radiometric ocean data. The SeaBASS database includes the NASA bio-Optical Marine Algorithm Dataset (NOMAD) (https://seabass.gsfc.nasa.gov/wiki/NOMAD), which contains the values of the bio-optical parameters required for this study, namely Chl-a and SPM concentrations and the a_{CDOM} coefficient at 443 nm. Since the SeaBASS dataset is built upon data collected over the global ocean (i.e., open and coastal ocean), only data acquired within 50 km from the coastlines have been selected for the current study. The CCRR dataset has been built specifically for the analysis of coastal areas. Similarly as for the SeaBASS dataset, only the Chl-a, SPM and a_{CDOM} parameters acquired within 50 km off the coastlines have been used here. Figure 2 shows the world map of the coastal sites within the SeaBASS and CCRR datasets selected for the purpose of this study. It could be observed that the selected measurements are representative of the coastal waters at a global scale.

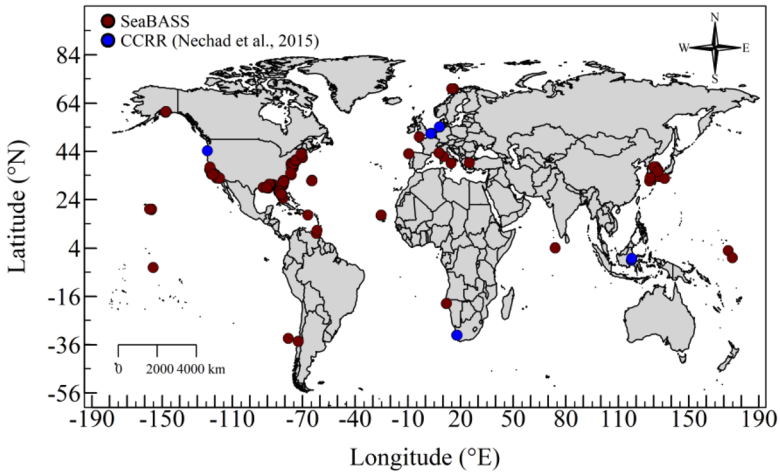

Fig. 2. World map of the coastal sites that have been selected for this study based on the SeaBASS [14] and the CCRR [15] datasets (i.e., sites are within 50 km off the coastlines). The SeaBASS and CCRR datasets are represented in red and blue respectively.

Optics EXPRESS

A straightforward statistical analysis of the overall coastal dataset used here (i.e., SeaBASS and CCRR) has been carried out to identify the values of the Chl-a concentration, SPM concentration and $a_{CDOM}(443\,nm)$ that are the most relevant to use as inputs of the radiative transfer model. The statistical parameters related to these variables are reported in Table 2.

Table 2. Statistical parameters related to the Chl-a, SPM and $a_{CDOM}(443\,nm)$ variables estimated through the analysis of the SeaBASS and CCRR databases for which only data measured within 50 km from the coastlines were considered: the number of samples N and the values of the minimum, maximum, mean, median, standard deviation σ and of the coefficient of variation (i.e., the ratio σ/mean in %) of each variable are reported. "NA" indicates that values are not available from the databases.

Variable	Dataset	N	Min	Max	Mean	Median	σ	Coef. variation (%)
Chl-a (mg m^{-3})	SeaBASS	319	0.05	48.99	3.89	1.57	6.23	160
	CCRR	47	0.28	43.1	5.48	3.06	7.52	137
	SeaBASS + CCRR	366	0.05	48.99	4.09	1.77	6.40	156
SPM (g m^{-3})	SeaBASS	NA	NA	NA	NA	NA	NA	NA
	CCRR	38	1.26	118	20	9.07	25	122
a_{CDOM} (m^{-1})	SeaBASS	330	0.006	0.88	0.16	0.07	0.18	110
	CCRR	NA	NA	NA	NA	NA	NA	NA

The number of samples that is related to Chl-a concentration and $a_{CDOM}(443\,nm)$ measurements is much greater (by a factor of 9) than the number of SPM concentrations because Chl-a and a_{CDOM} were systematically measured as a requirement to build the SeaBASS database. The values of the coefficients of variation are systematically greater than 110% for each variable, thus illustrating the strong variability observed in coastal zones. As a result, the use of median values appears to be more relevant than the average values to minimize the influence of pronounced local or regional coastal features.

Histograms of variation of each variable are shown in Fig. 3. Most of the a_{CDOM} values are lower than 0.4 m^{-1}. The Chl-a concentration values are mainly distributed below 10 mg m^{-3} while a wider heterogeneity of the SPM values is observed as a result of the significant variability encountered in coastal ecosystems. However, it is interesting to highlight that almost all the values of SPM concentrations remain below 100 g m^{-3} except for one sample. In addition, a maximum value of SPM of 100 g m^{-3} is consistent with coastal observations performed in other areas by previous studies [16–20]. Therefore, the upper limit of the range of variation of the SPM values used for the radiative transfer computations performed in this paper is set to 100 g m^{-3}.

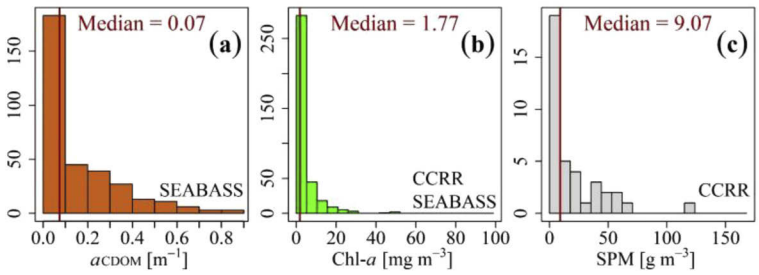

Fig. 3. Histograms of variation of the Chl-a concentration, the SPM concentration and $a_{CDOM}(443\,nm)$ over the SeaBASS and CCRR datasets. The red vertical line indicates the median value for each variable.

Optics EXPRESS

2.3. Radiative transfer modelling

The top of atmosphere upwelling radiance that could be potentially measured by a satellite ocean color sensor at night has been simulated using the so-called radiative transfer model Ocean Successive Orders with Atmosphere – Advanced (OSOAA) [21]. The OSOAA model is able to compute the angular distribution of the upward radiance for the ocean-atmosphere system taking into account a rough sea surface. The radiative transfer equation is solved using the successive orders of scattering method and the Stokes parameters formalism, thus allowing a simulation of both the radiance and the polarization state of light. The bio-optical properties of various types of aerosols and hydrosols are taken into account as inputs of the model. The hydrosols consist of phytoplankton-like particles (characterized by the chlorophyll *a* concentration), SPM and a_{CDOM}. The OSOAA model has been designed to perform simulations in the visible and near infrared spectral range, namely from 400 nm to 800 nm. The reader is referred to Chami et al. [21]. for more details about the description of the OSOAA model. Based on the statistical analysis of the in-situ bio-optical datasets used here (Table 2) and as mentioned in Section 2.2, the selection of the median values of Chl-a concentration, SPM concentration and $a_{CDOM}(443\,nm)$, namely 1.8 mg m^{-3}, 9 g m^{-3} and 0.07 m^{-1} respectively, is relevant to define a benchmark radiative transfer simulation, so-called the "median case". Such a median case could be representative of a wide variety of coastal waters. The overall inputs used as a benchmark for modelling the upward radiance are reported in Table 3. The calculations were carried out for the entire spectral range of OSOAA (400 nm to 800 nm) by steps of 5 nm. The phase functions of hydrosols are obtained from Mie theory using two different values of the refractive index for phytoplankton-like particles and SPM particles. A Junge power law size distribution (i.e., Junge exponent, minimum radius r_{min} and r_{max}) is used for both types of hydrosols. Note that Shettle and Fenn's coastal model has been used to determine the aerosol optical properties [22].

The outputs of the simulations consist of the angular distribution of the upward radiance at the top of atmosphere. Since the radiances that are initially computed by the OSOAA model are normalized to a value of an extraterrestrial incident irradiance of π (unit sr^{-1} μm^{-1}), the initial simulated radiances have been multiplied by the ratio EL_{TOA}/π to account for the moonlight incident illumination, thus providing values of the radiance in geophysical units (in W m^{-2} sr^{-1} μm^{-1}). Note that OSOAA simulations performed for daytime conditions under a sunlight illumination would provide values about 5.10^5 times greater than those obtained under a moonlight illumination. Such a difference corresponds in fact to the ratio between the solar and the lunar irradiance as mentioned in Section 2.1. In addition, the convolution of the OSOAA hyperspectral radiances with the spectral response function (SRF) of the panchromatic DNB of the VIIRS sensor, referred to as PAN(LTOA) (in W m^{-2} $sr^{-1}\mu m^{-1}$), is carried out as follows [Eq. (3)]:

$$PAN(LTOA) = \frac{\sum_{\lambda i} L_{TOA}(\lambda_i) \times SRF(PAN(\lambda_i))}{\sum_{\lambda i} SRF(PAN(\lambda_i))} \quad (3)$$

where λ is the wavelength, L_{TOA} is the top of atmosphere radiance, $SRF(PAN(\lambda_i))$ is the SRF of the panchromatic DNB of the VIIRS sensor [8] (Fig. 4).

As mentioned earlier in the paper (Section 1), it should be noted that the SRF of the DNB of the VIIRS sensor is primarily used in this study since this sensor is currently the only on-orbit ocean color sensor that is able to accurately measure extremely low signals, such as those encountered for moonlight illuminations. However, it should be highlighted that the convolution of the OSOAA radiances with the SRF of the DNB is made only over the OSOAA spectral range (400 nm - 800 nm) despite the fact that VIIRS sensor is able to measure at wavelengths greater than 800 nm (Fig. 4). This is not a major issue for the objectives of this study because the optical signature of the SPM remains highly pronounced in the visible spectrum, especially between 500 nm and 800 nm; this is one reason for which most of the ocean color sensors are equipped with a

Optics EXPRESS

Table 3. Parameters used as inputs in the OSOAA radiative transfer model to define the benchmark simulation. S_{CDOM} is the spectral slope of a_{CDOM} coefficient, r_{min} and r_{max} are the minimum and maximum radius of the Junge size distribution of the hydrosols respectively, J is the Junge exponent of the size distribution, AOT is the aerosol optical thickness, EL_{TOA} is the lunar extraterrestrial irradiance, θ_L is the Lunar zenith incident angle. The literature references that are used to justify the values of certain inputs are mentioned wherever possible. The values of Chl-a, SPM and a_{CDOM}(443 nm) reported in this table are the median values (so-called "median case") calculated from the in-situ datasets (Table 2).

Input parameters		Values	Literature reference
Chl-a (mg m^{-3})		1.8	SeaBASS and CCRR database [14,15]
SPM (g m^{-3})		9	CCRR database [15]
a_{CDOM}(443 nm) (m^{-1})		0.07	SeaBASS database [14]
S_{CDOM} (m^{-1})		0.0176	Babin et al. [16,17]
Complex refractive index	Phytoplankton	1.05-0.00i	-
	SPM	1.15-0.00i	-
Junge exponent J (size distribution)		4	-
Minimum radius (r_{min}, µm)		0.01	-
Maximum radius (r_{max}, µm)		200	-
Aerosol model	Coastal with humidity of 90%	C90	Shettle and Fenn [22]
Aerosol Optical Thickness (AOT)		0.2	-
Wind speed (m s^{-1})		5	Harmel and Chami [23]
Lunar irradiance EL_{TOA} at 600 nm (W m^{-2} μm^{-1})		4 10^{-3}	
Lunar zenith incident angle θ_L (°)		30	-
Seabed depth (m)		50	-
Seabed composition		Sand	-

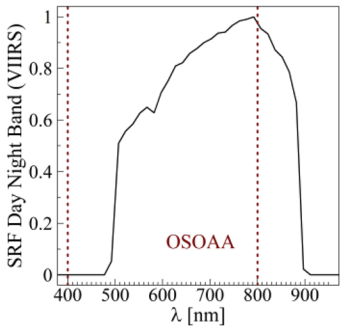

Fig. 4. Spectral response function (SRF) of the Day-Night Band (DNB) of the VIIRS satellite sensor [8]. The spectral range of the simulations performed by OSOAA model is also shown (red vertical lines).

spectral band centered around 620 nm that is dedicated to deriving the SPM concentrations in coastal areas.

The simulations are carried out for relative difference azimuth angles, referred to as ϕ_{OSOAA}, ranging from 0 to 180° by steps of 10°. Note that the relative difference azimuth angle is defined as the difference between the azimuth angle of the Moon and the azimuth angle of the satellite sensor. The so-called principal plane observation is defined as the plane composed of

Optics EXPRESS

the two half-planes for which the values of ϕ_{OSOAA} are 0° and 180°. It should be noted that the geometrical convention that is used by the OSOAA model is defined such that the value of ϕ_{OSOAA} of 0° corresponds to an observation made in the Moon specular half-plane (i.e., the moon and the satellite sensor are in two opposite planes). The specular half-plane is also the half-plane containing the moonglint. A value of ϕ_{OSOAA} of 180° corresponds to an observation made in the anti-specular half-plane (i.e., the Moon and the satellite sensor are located in the same plane), which is in fact the backscattering plane. The output radiances calculated by the OSOAA model are provided for viewing zenith angles, referred to as θ_v, ranging from 0 to 80° by steps of 1.5°. However, unless specified, most of the results that correspond to an observation made in the specular plane are shown for the nadir viewing zenith angle (i.e., θ_v=0°).

3. Results

Figure 5(a) shows the values of the simulated top of atmosphere radiances in the panchromatic DNB PAN(L_{TOA}) [Eq. (3)] in the specular plane (i.e., ϕ_{OSOAA}=0°) for a nadir viewing zenith angle (i.e., θ_v=0°) and for SPM concentrations ranging from 1 to 100 g m^{-3}. The computations are carried out using the benchmark parameters listed in Table 3 in the case of a full moon incident illumination. It should be noted that the values of Chl-a concentration and a_{CDOM} are set to their median values (Table 2 and Fig. 3) for all the computations presented here.

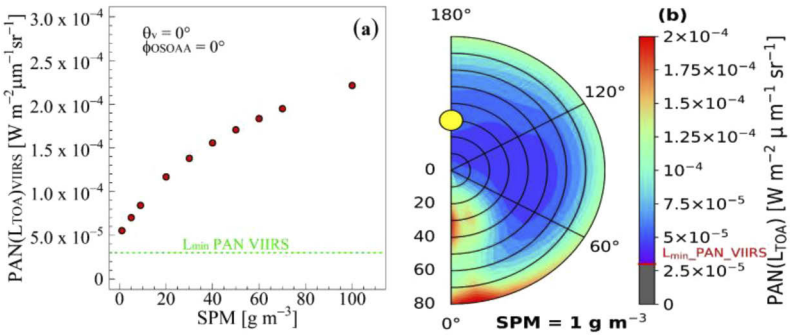

Fig. 5. (a) Variation of the simulated values of the top of atmosphere radiances PAN(L_{TOA}) (in W m^{-2} µm^{-1} sr^{-1}) [(Eq. (3)] with the SPM concentrations in the specular plane (i.e., ϕ_{OSOAA}=0° and θ_v=0°) for a full moon incident illumination. The simulations are carried out for the benchmark parameters reported in Table 3 and for the spectral response function of the VIIRS DNB. The minimum radiance value that is measurable by the VIIRS sensor in the DNB ($L_{min\_PAN\_VIIRS}$) is mentioned as well (green line), (b) polar diagram of the angular variation of PAN(L_{TOA}) for SPM=1 mg m^{-3}; the relative azimuth angle ϕ_{OSOAA} is represented by straight lines while the viewing zenith angle is represented by circles. The position of the Moon (ϕ_{OSOAA}=180° and θ_L=30°) is indicated by the yellow circle. A grey color is used in the color bar when PAN(L_{TOA}) is lower than $L_{min\_PAN\_VIIRS}$.

As expected, the values of PAN(L_{TOA}) increase with the turbidity as a result of the increased contribution of the SPM to the light scattering processes in the ocean. More interestingly, PAN(L_{TOA}) is systematically greater than the minimum radiance value that could be measured by VIIRS sensor, namely $L_{min\_PAN\_VIIRS}$ (3.10^{-5} W m^{-2} µm^{-1} sr^{-1}, [7]). In particular, PAN(L_{TOA}) is higher than $L_{min\_PAN\_VIIRS}$ by a factor of 1.8 (5.5 10^{-5} W m^{-2} µm^{-1} sr^{-1}) and 7.5 (2.2 10^{-4} W m^{-2} µm^{-1} sr^{-1}) from clear (SPM=1 g m^{-3}) to highly turbid (SPM=100 g m^{-3}) waters. Therefore, not only could the SPM concentrations be observable from a VIIRS-like satellite sensor at night, including in clear waters, but also the top of atmosphere radiances PAN(L_{TOA}) are sufficiently sensitive to the SPM concentrations to make the satellite radiances potentially exploitable for a quantitative estimation of the SPM concentration at night. Note that a similar conclusion was

Optics EXPRESS

obtained when a higher value of the real part refractive index of the hydrosols, namely 1.20, was tested in the computations; the latter point was expected since highly refractive hydrosols lead to an increase of the light scattering, thus also increasing the value of the water leaving radiance and the subsequent top of atmosphere radiance. The variation of PAN(L_{TOA}) values with the observation geometry shows that the presence of SPM could be detected in clear waters at night whatever the azimuth and viewing zenith angle [Fig. 5(b)]. Polar diagrams like the one shown in Fig. 5(b) are relevant to identify the least favorable geometrical configuration for observing the SPM at night. It could be noticed here that the minimum values of the radiances PAN(L_{TOA}), which are thus the values the closest to the minimum radiance measureable by VIIRS ($L_{min\_PAN\_VIIRS}$), are not located in the principal plane geometry but they are found within a relative azimuth range ϕ_{OSOAA} from 60° to 120° when the viewing zenith angle θ_v ranges from 5° to 55° [Fig. 5(b)]. Similar conclusions as those drawn from Fig. 5(b) were obtained when a value of 60° is used for the Lunar incident zenith angle θ_L except for a small geographic area located in the range of ϕ_{OSOAA} between 60° and 90° when θ_v values are between 0° and 20°. For such a small area, the minimum value of PAN(L_{TOA}) (2.8 10^{-5} W m^{-2} μm^{-1} sr^{-1}) is slightly lower than $L_{min\_PAN\_VIIRS}$ (3 10^{-5} W m^{-2} μm^{-1} sr^{-1}), thus meaning that the detection of SPM is not theoretically feasible for clear waters only (SPM=1 g m^{-3}). However, it was observed that the SPM detection becomes feasible again for such geometry for SPM values greater than 9 g m^{-3}.

The sensitivity of the results shown in Fig. 5 to the size distribution of the hydrosols has been examined. For that purpose, the value of the Junge exponent J of the size distribution was varied from 3.5 to 4.5 (Fig. 6). Typically, lower values of the Junge exponent (e.g., J=3.5) means that a higher amount of large size hydrosols are present while increased values of J (e.g., J=4.5) means that the contribution of small size hydrosols is higher within the overall population of hydrosols.

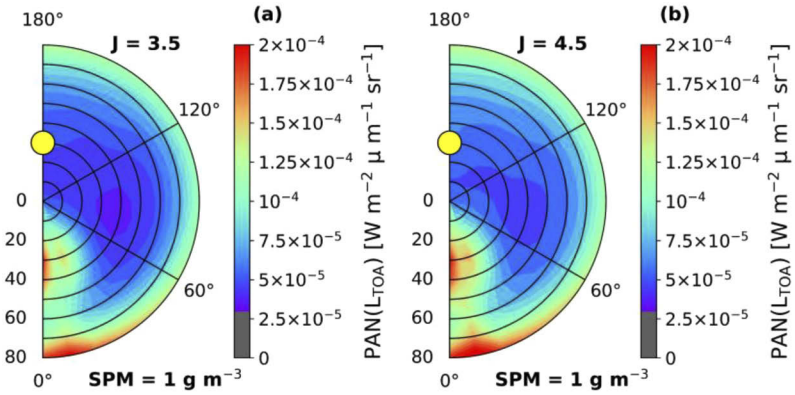

Fig. 6. Similar to Fig. 5(b) but for various values of the Junge exponent J of the size distribution of the hydrosols, namely (a) J=3.5 and (b) J=4.5.

Figure 6 shows that the values of PAN(L_{TOA}) for SPM=1 g m^{-3} remains systematically higher than $L_{min\_PAN\_VIIRS}$ for all geometries whatever the values of J. Note that the values observed in the area characterized by a value of ϕ_{OSOAA} between 60° and 90° and a value of θ_v between 30° and 45° are just slightly greater than the minimum detectable radiance when J=3.5. However, since the value of PAN(L_{TOA}) increases with SPM concentrations, the SPM detection will be more effective in waters showing SPM concentrations greater than 1 g m^{-3}, which represent the large majority of the waters observed in coastal zones. It should also be noted from Fig. 6 that the top of atmosphere radiances calculated for J=3.5 are slightly weaker than those observed for J=4.5 over all the geometries. A decrease of PAN(L_{TOA}) with lower values of J is expected because of the influence of the hydrosol size on the phase function of the hydrosols. Large size hydrosols induce a more pronounced forward peak of the phase function due to the diffraction

Optics EXPRESS

process, thus resulting in a decrease of the backscattered light that leads to a decrease of the oceanic radiance reaching the satellite sensor.

The influence of the atmospheric turbidity on the panchromatic top of atmosphere radiances has been studied based on the benchmark simulation parameters (Fig. 7). The values of the aerosol optical depth (AOT) were varied from 0.1 to 0.5, which roughly correspond to horizontal visibilities of 50 km and 8 km respectively. It is interesting to observe that the previous conclusions concerning the feasibility of detecting SPM at night whatever the observation geometry remain true for a clear atmosphere [Fig. 7(a)]. The oceanic radiation is thus detectable from a VIIRS-like satellite sensor despite the extremely low levels of signals exiting the ocean in the clear water case. In addition, Fig. 7(a) implies that more turbid waters (SPM > 1 g m^{-3}) could be effectively observed under a full moon incident illumination. Because a higher aerosol loading leads to an increase of PAN(L_{TOA}) due to the higher atmospheric light scattering, values of PAN(L_{TOA}) greater than $L_{min\_PAN\_VIIRS}$ is naturally expected for the case AOT=0.5 [Fig. 7(b)].

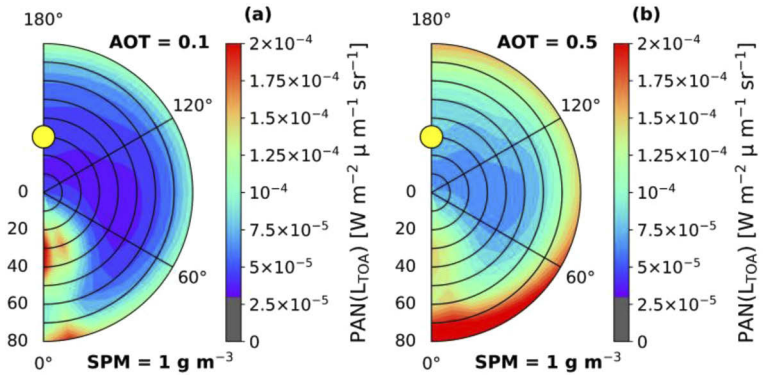

Fig. 7. Similar as Fig. 5(b) but for various values of the aerosol optical thickness (AOT), namely (a) AOT=0.1 and (b) AOT=0.5.

4. Discussion

The top of atmosphere radiance has been simulated using radiative transfer modelling to investigate the feasibility of detecting and quantifying the concentrations of suspended matter in coastal waters at night for a full moon incident illumination. The use of the OSOAA radiative transfer model for that purpose is relevant due to its ability to account for the propagation of the light within the coupled ocean-atmosphere system for various oceanic and atmospheric optical features. Note that OSOAA model has recently been successfully used to check the radiometric calibration of one satellite ocean color sensor, namely the New AstroSat Optical Modular Instrument (NAOMI) mounted on the Vietnamese VNREDSat-1 satellite, [24], thus confirming its appropriate use as a forward model for the current study.

Careful attention has been paid to introduce inputs parameters within the OSOAA simulations as consistent as possible with real-world observations. As examples, in-situ bio-optical datasets that are appropriate for coastal areas, namely the SeaBASS and CCRR datasets, were used to provide realistic values of the Chl-a, SPM and a_{CDOM} parameters. The results presented in Section 3 interestingly revealed that although the amplitude of the signal reaching a satellite sensor is extremely weak, typically about 5 10^{-5} W m^{-2} µm^{-1} sr^{-1}, the high performance of both the spectral and radiometric specifications of the VIIRS ocean color sensor, namely its spectral Day-Night Band and its minimum detectable radiance (3 10^{-5} W m^{-2} µm^{-1} sr^{-1}), makes it possible to measure the optical signature of the hydrosols from space under moonlight conditions.

Optics EXPRESS

The prelaunch characteristics of the spectral response function (SRF) of the DNB have been used in this paper (Fig. 4). Liao et al. [25] performed a rigorous analysis of the on-orbit performance of the VIIRS sensor. A deviation of the SRF of the DNB was identified in comparison to the prelaunch specifications; such a deviation consists of a spectral shift of the maximum value of the SRF toward shorter wavelengths, namely from 780 nm to 700 nm. Such a spectral shift should not change the conclusions drawn in the current paper because the amplitude of the water leaving radiance signal induced by the occurrence of SPM is more pronounced at 700 nm compared to 780 nm owing to the strong absorption caused by the water molecules for increasing wavelengths.

The fact that the a_{CDOM} values did not vary in the simulations should not significantly alter the conclusions drawn from the results presented here because the optical influence of CDOM matter is weak in the spectral range that is covered by the VIIRS DNB spectral band (λ>500 nm, Fig. 4). Similarly, the fact that the main absorption peak of Chl-a around 440 nm is out of the DNB contributes to minimize the influence of Chl-a turbidity on PAN(L_{TOA}). However, the secondary absorption peak of Chl-a around 676 nm could possibly influence PAN(L_{TOA}) values especially for a high Chl-a turbidity. Therefore, additional simulations of PAN(L_{TOA}) similar to those shown in Fig. 5(a) were performed for various Chl-a concentrations, namely from 0.5 mg m^{-3} to 10 mg m^{-3}. Note that an upper Chl-a limit of 10 mg m^{-3} is consistent with the variability observed within the bio-optical datasets (see the coefficient of variation in Table 2). It was observed that values of PAN(L_{TOA}) (i) remain systematically higher than $L_{min\_PAN\_VIIRS}$ whatever the Chl-a turbidity, (ii) remain significantly sensitive to SPM concentrations, and (iii) decrease with Chl-a turbidities. Note, however, that the decrease of PAN(L_{TOA}) remains lower than 10% from the value obtained for the median case (Chl-a=1.8 mg m^{-3}). Therefore, the feasibility of detecting SPM from the panchromatic band of a VIIRS-like sensor under night conditions remains true for values of Chl-a concentration lower or higher than the median value used in this study.

Shi and Wang [9] recently illustrated the potential of the VIIRS DNB to characterize the ocean front of suspended sediment and to visualize coastal ocean dynamics at night near the full moon phase. However, these authors highlighted the difficult task of quantitatively deriving the ocean radiance contributions essentially because of the very low signals measured by the satellite. The current study provides quantitative values of the radiances reaching the satellite sensor for various oceanic turbidities, including in clear waters [Fig. 5(a)], for various phase functions of hydrosols (Fig. 6) and for various atmospheric turbidities, including for a clear atmosphere (Fig. 7). In particular, our results showed that the top of atmosphere radiances are significantly greater than the minimum detectable VIIRS radiance $L_{min\_PAN\_VIIRS}$, typically by a factor of 2 for moderately turbid waters (SPM = 20 g m^{-3}) up to a factor of 4 for turbid waters (SPM=100 g m^{-3}) [Fig. 5(a)]; note that waters for which SPM > 20 g m^{-3} represent a wide variety of the observations made in coastal zones at a global scale, including estuaries [26]. Although the development of robust atmospheric correction algorithms remains a challenging task when dealing with satellite observations over coastal waters, the exploitation of top of atmosphere radiances which are greater by a factor of 2 to 4 than the minimum detectable radiance of a given sensor should enable the atmospheric correction methods to retrieve SPM concentrations with acceptable accuracy. Note that although the topic of the atmospheric correction is beyond the scope of this study, the values provided here could be used with relevance to optimize the development of atmospheric correction algorithms that would be dedicated to night satellite measurements. Similarly, although it is not the scope of this study to treat the inverse problem of the ocean color, the significant sensitivity of PAN(L_{TOA}) with the SPM turbidity, as observed in Fig. 5(a), could be an interesting lead to explore for deriving SPM concentrations from satellite panchromatic data under night conditions, for example using either an empirical-based approach or a semi-analytical approach based on radiative transfer modelling.

Optics EXPRESS

Because the best night observations for the ocean monitoring are available for full moon conditions due to the maximum incident lunar illumination of the earth, most of the previous studies [8,9] focused on examining the possibilities of using the VIIRS DNB for such a full moon phase. However, the full moon phase only represents 1 night of measurements over the course of the lunar cycle, which is clearly not sufficient to properly investigate the strong dynamical processes involving SPM in coastal environments. Therefore, the possibility of observing the SPM variability for a higher number of nights over the course of the lunar cycle is examined here. For that purpose, the top of atmosphere radiances PAN(L_{TOA}) are simulated for various fractions F of the extraterrestrial lunar irradiance EL_{TOA} ranging from 0% to 100%. Figure 8 shows the variation of PAN(L_{TOA}) with respect to the amplitude of the Lunar irradiance EL_{TOA} for clear waters conditions (SPM=1 g m^{-3}) in the specular plane observation (i.e., ϕ_{OSOAA}=0° and θ_v=0°).

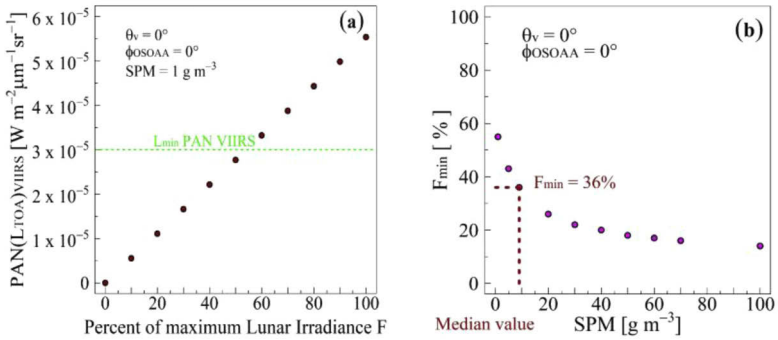

Fig. 8. (a) Variation of the top of atmosphere radiance PAN(L_{TOA}) with the fraction F (in %) of the lunar extraterrestrial irradiance EL_{TOA}. A value of F of 100% represents the full moon illumination. The simulations were carried out using the benchmark parameters listed in Table 3 except for the value of SPM which is 1 g m^{-3} here (clear water). The observation geometry is the specular plane (ϕ_{OSOAA}=0°) at a nadir viewing angle (θ_v=0°). The minimum radiance value that is measurable by the VIIRS sensor in the DNB ($L_{min\_PAN\_VIIRS}$) is also mentioned (green line), (b) variation of the minimum value of F (noted F_{min}) from which PAN(L_{TOA}) is higher than $L_{min\_PAN\_VIIRS}$ with SPM concentrations.

It is interesting to observe [Fig. 8(a)] that the value of PAN(L_{TOA}) remains greater than the minimum detectable radiance $L_{min\_PAN\_VIIRS}$ when the fraction F decreases from 100% to 60%. This means that the near full moon phase is not the only condition for which a VIIRS-like sensor could potentially detect the presence of SPM at night in clear waters. The minimum value of F from which PAN(L_{TOA}) is higher than $L_{min\_PAN\_VIIRS}$ is hereafter referred to as F_{min}; F_{min}=60% in the case of Fig. 8(a). The value of F_{min} significantly decreases with turbidity, typically from 60% (clear waters) to 10% (turbid waters) in the specular plane [Fig. 8(b)]. Such a decrease is expected as a result of the higher amplitude of the water leaving radiance with turbidity, which implies the requirement of lower values of the incident illumination F of the ocean by the moonlight. It should be highlighted that the lower F_{min}, the greater the number of potential nights for observing SPM over the course of the lunar cycle. Note that the value of F_{min} is 36% for the median value of the SPM concentration (9 g m^{-3}). Therefore, a reduction of 64% (i.e., from 100% to 36%) of the full moon incident illumination might allow observation of moderately turbid waters (SPM=9 g m^{-3}). Similarly, a reduction of 90% of full moon light (i.e., from 100% to 10%) might allow the detection of highly turbid waters, such as those found in estuaries (SPM > 70 g m^{-3}). The simulations performed at all the observation geometries confirm the decrease of F_{min} with turbidity for other planes than the specular plane (Fig. 9). The minimum values of F_{min} over all the geometries are observed for a relative azimuth angle around 10°, which is close

Optics EXPRESS

to the specular plane. Knowledge of the full spatial variation of F_{min} is of primary importance to identify the most favorable configuration of observation for which a satellite sensor should be able to acquire data to increase the frequency of night detection of the SPM concentration.

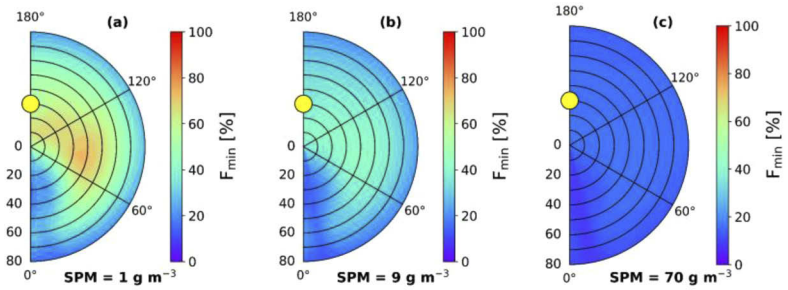

Fig. 9. Spatial variation of the fraction F_{min} over the observation geometries for various oceanic turbidities: (a) SPM=1 g m^{-3}, (b) SPM=9 g m^{-3}, (c) SPM=70 g m^{-3}. F_{min} is the minimum value of F from which PAN(LTOA) is higher than $L_{min\_PAN\_VIIRS}$.

The relationship that exists between the lunar extraterrestrial irradiance EL_{TOA} and the lunar phase angle (Fig. 1) could be used to relate PAN(L_{TOA}) with the lunar phase angle φ_{Lunar} [Fig. 10(a)]. This is possible because the radiances calculated by OSOAA, which are originally provided for an extraterrestrial irradiance value of π, are converted into geophysical units (W m^{-2} sr^{-1} μm^{-1}) using EL_{TOA} as mentioned in Section 2.3. As an example, the value of φ_{Lunar} below which the amplitude of PAN(L_{TOA}) is greater than $L_{min\_PAN\_VIIRS}$ is 32° for clear waters (SPM=1 g m^{-3}) in the specular plane [Fig. 10(a)]. Then, it is possible to determine the total number of nights for which the SPM concentrations could be potentially detected over the course of the lunar cycle using Table 1 [Fig. 10(b)].

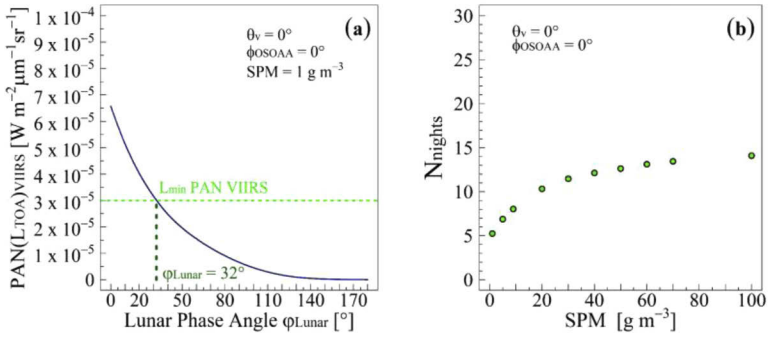

Fig. 10. (a) Relationship between the top of atmosphere radiance PAN(L_{TOA}) and the lunar phase angle φ_{Lunar} for a value of SPM of 1 g m^{-3} in the specular plane (ϕ_{OSOAA}=0° and θ_v=0°), (b) variation of the total number of nights N_{nights} for which the amplitude of the moon light illumination is sufficiently high to observe SPM as a function of the turbidity.

The most striking feature observed in Fig. 10(b) is that the amplitude of the Moon light illumination out of the full moon phase is sufficiently high to enable the detection of SPM concentrations for a high number of nights, typically up to 5 nights per month for clear waters and up to 15 nights per month for turbid waters over the course of the lunar cycle. As a comparison, the revisit period of the Multi-Spectral Instrument (MSI) on-board Sentinel 2 satellite (ESA), which is able to observe coastal zones at a high spatial resolution ranging from 10 m to 60 m, allows at best (i.e., cloud-free conditions) a number of daylight acquisitions of 6 images per

Optics EXPRESS

month (1 every 5 days). Therefore, our results show that the frequency of potential nighttime measurements of SPM using a VIIRS-like sensor to monitor the coastal rapid processes, such as rivers discharge or the sediment transport is at worse, similar as the current Sentinel 2/MSI sensor. The monitoring of rapid processes will be efficient because the nighttime data acquisitions are centered on the full moon and thus, acquisitions are carried out for successive nights before and after the full moon phase, which is convenient to study the SPM dynamics using remote sensing night data in addition to daylight acquisitions. Miller et al. [8] highlighted that the local nighttime overpass of the VIIRS sensor (typically around 01h30 am) allows lunar night observations for one-half of the entire lunar cycle. The quantitative analysis performed in the current study demonstrates that the sensitivity of the DNB is sufficient to exploit moonlight illumination during such 2 week period in order to determine the SPM concentrations.

5. Conclusion

In this paper, the panchromatic Day-Night Band and the radiometric specifications of the VIIRS ocean color sensor have been exploited to investigate the feasibility of performing nocturnal observations of the suspended matter in coastal waters. The radiative transfer modelling has been used to simulate the top of atmosphere radiances under various Moon incident illuminations. Special attention was paid to provide consistent and realistic values of the bio-optical parameters used as inputs of the model. In particular, in-situ datasets showing a high variability of coastal waters and which are publicly available were analyzed to set relevant values for describing the hydrosols optical properties and the water turbidity. The results revealed that quantitative observations of the SPM are systematically feasible at night for a wide variety of atmospheric and oceanic conditions (e.g., atmospheric turbidity, size of hydrosol, observation geometries), thus confirming the high performance of the VIIRS sensor. While most of the previous studies focused on night applications of VIIRS observations near the full moon phase [8,9], this paper also focused on analyzing the capabilities of SPM detection over the course of the entire lunar cycle. It was shown that the frequency of satellite night acquisitions over the lunar cycle (29.5 nights) is between 5 to 15 nights depending on the turbidity of the water. Therefore, nighttime satellite observations combined with daylight measurements should greatly improve the monitoring of SPM in coastal areas, which is of great interest for many applications such as modelling the sediment transport, understanding the ecosystems structure and functioning or anticipating dredging activities in areas affected by coastal environmental changes. The results outlined in this paper could be further used for the development and/or optimization of robust atmospheric correction algorithms to derive SPM concentrations at night, which remain a challenging task due to the extremely low level signals involved.

Funding

Thales Alenia Space (TAS/OCA #193878).

Acknowledgments

The authors are grateful to the NASA SIMBIOS Program (NRA-96-MTPE-04 and NRA-99-OES-09) for the availability of the SEABASS bio-optical database. We are grateful as well to all the contributors and in-situ data providers of the CoastColour project, which was funded by the European Space Agency, for making available the CoastColour Round Robin (CCRR) dataset used in this study. We would like to thank the Centre National d'Etudes Spatiales (CNES-France) for the maintenance and the online distribution of the OSOAA radiative transfer model (https://github.com/CNES/RadiativeTransferCode-OSOAA) and Bruno Lafrance from the CS-SI Company (Toulouse, France) for helpful discussions about the use of the OSOAA model. The authors wish to thank Thierry Lanz and Martin Vannier from the Observatoire Côte d'Azur

Optics EXPRESS

(France) and Thierry Viard from Thales Alenia Space for providing all facilities to perform the "LUMES" project in the frame of the Laboratoire Commun "LOSCA" (partnership between the Observatoire Côte d'Azur and Thales Alenia Space). The authors are grateful to Timothy Kendall for the english editorial corrections. The authors wish to thank the reviewers for their relevant comments and suggestions.

Disclosures

The authors declare no conflicts of interest.

References

1. S. B. Hooker and W. E. Esaias, "An overview of the SeaWiFS Project," Trans., Am. Geophys. Union **74**(21), 241–246 (1993).
2. W. E. Esaias, M. R. Abbott, I. Barton, O. B. Brown, J. W. Campbell, K. L. Carder, D. K. Clark, R. L. Evans, F. E. Hodge, H. R. Gordon, W. P. Balch, R. Letelier, and P. J. Minnet, "An overview of MODIS capabilities for ocean science observations," IEEE Trans. Geosci. Electron. **36**(4), 1250–1265 (1998).
3. C. Donlon, B. Berruti, A. Buongiorno, M. H. Ferreira, P. Femenias, J. Frerick, P. Goryl, U. Klein, H. Laur, C. Mavrocordatos, J. Nieke, H. Rebhan, B. Seitz, J. Stroede, and R. Sciarra, "The Global Monitoring for Environment and Security (GMES) Sentinel-3 mission," Remote Sens. Environ. **120**, 37–57 (2012).
4. ACE Ocean Science Team. ACE Ocean Biology White Paper, Appendix. http://neptune.gsfc.nasa.gov/uploads/files/ACE−ocean−white−paper−appendix−5Mar10.doc (2010).
5. IOCCG, *Mission Requirements for Future Ocean Colour Sensor*, C. McClain and G. Meister eds., Reports of International Ocean-Color Coordinating Group, No. 13, IOCCG, Dartmouth, Canada, doi: 10.25607/OBP-104 (IOCCG, 2012), pp. 106.
6. T. F. Lee, S. D. Miller, F. J. Turk, C. Schueler, R. Julian, S. Deyo, P. Dills, and S. Wang, "The NPOESS/VIIRS day/night visible sensor," Bull. Am. Meteorol. Soc. **87**(2), 191–200 (2006).
7. H. Oudrari, J. McIntire, X. Xiong, J. Butler, B. Efremova, Q. Ji, S. Lee, and T. Schwarting, "JPSS-1 VIIRS pre-launch radiometric performance," Proc. SPIE **9607**, 960710 (2015).
8. S. D. Miller, W. Straka, S. P. Mills, C. D. Elvidge, T. F. Lee, J. Solbrig, A. Walther, A. K. Heidinger, and S. C. Weiss, "Illuminating the capabilities of the Suomi National Polar-Orbiting Partnership (NPP) Visible Infrared Imaging Radiometer Suite (VIIRS) day/night band," Remote Sens. **5**(12), 6717–6766 (2013).
9. W. Shi and M. Wang, "Ocean Dynamics Observed by VIIRS Day/Night Band Satellite Observations," Remote Sens. **10**(2), 76 (2018).
10. H. H. Kieffer and T. C. Stone, "The Spectral Irradiance of the Moon," Astron. J. **129**(6), 2887–2901 (2005).
11. T. C. Stone, H. H. Kieffer, and K. J. Becker, "Modeling the radiance of the moon for on-orbit calibration," Proc. SPIE **5151**, 463–470 (2003).
12. G. Thuillier, M. Hersé, D. Labs, T. Foujols, W. Peetermans, D. Gillotay, P.C. Simon, and H. Mandel, "The Solar Spectral Irradiance from 200 to 2400 nm as Measured by the SOLSPEC Spectrometer from the Atlas and Eureca Missions," Sol. Phys. **214**(1), 1–22 (2003).
13. S. D. Miller and R. E. Turner, "A dynamic lunar spectral irradiance data set for NPOESS/VIIRS day/night band nighttime environmental applications," IEEE Trans. Geosci. Electron. **47**(7), 2316–2329 (2009).
14. P. J. Werdell and S. W. Bailey, "An improved in-situ bio-optical data set for ocean color algorithm development and satellite data product validation," Remote Sens. Environ. **98**(1), 122–140 (2005).
15. B. Nechad, K. Ruddick, T. Schroeder, K. Oubelkheir, D. Blondeau-Patissier, N. Cherukuru, V. Brando, A. Dekker, L. Clementson, A. C. Banks, S. Maritorena, P. J. Werdell, C. Sá, V. Brotas, I. Caballero de Frutos, Y. H. Ahn, S. Salama, G. Tilstone, V. Martinez-Vicente, D. Foley, M. McKibben, J. Nahorniak, T. Peterson, A. Siliò-Calzada, R. Röttgers, Z. Lee, M. Peters, and C. Brockmann, "CoastColour Round Robin data sets: a database to evaluate the performance of algorithms for the retrieval of water quality parameters in coastal waters," Earth Syst. Sci. Data **7**(2), 319–348 (2015).
16. M. Babin, D. Stramski, G. M. Ferrari, H. Claustre, A. Bricaud, G. Obolensky, and N. Hoepffner, "Variations in the light absorption coefficients of phytoplankton, nonalgal particles, and dissolved organic matter in coastal waters around Europe," J. Geophys. Res.: Oceans **108**(C7), 3211 (2003).
17. M. Babin, A. Morel, V. Fournier-Sicre, F. Fell, and D. Stramski, "Light scattering properties of marine particles in coastal and open ocean waters as related to the particle mass concentration," Limnol. Oceanogr. **48**(2), 843–859 (2003).
18. G. Tilstone, S. Peters, H. Van Der Woerd, M. Eleveld, K. Ruddick, W. Schönfeld, H. Krasemann, V. Martinez-Vicente, D. Blondeau-Patissier, P. V. Jorgensen, R. Rottgers, and K. Sorensen, "Variability in specific-absorption properties and their use in a semi-analytical ocean colour algorithm for MERIS in North Sea and Western English Channel Coastal Waters," Remote Sens. Environ. **118**, 320–338 (2012).
19. B. Lubac and H. Loisel, "Variability and classification of remote sensing reflectance spectra in the eastern English Channel and southern North Sea," Remote Sens. Environ. **110**(1), 45–58 (2007).

Optics EXPRESS

20. S. B. Wozniak, D. Stramski, M. Stramska, R. A. Reynolds, V. M. Wright, E. Y. Miksic, M. Cichocka, and A. M. Cieplak, "Optical variability of seawater in relation to particle concentration, composition, and size distribution in the nearshore marine environment at Imperial Beach, California," J. Geophys. Res. **115**(C8), C08027 (2010).
21. M. Chami, B. Lafrance, B. Fougnie, J. Chowdhary, T. Harmel, and F. Waquet, "OSOAA: a vector radiative transfer model of coupled atmosphere-ocean system for a rough sea surface application to the estimates of the directional variations of the water leaving reflectance to better process multi-angular satellite sensors data over the ocean," Opt. Express **23**(21), 27829–27852 (2015).
22. E. P. Shettle and R. W. Fenn, "Models for the aerosols of the lower atmosphere and the effect of humidity variations on their optical properties," in *Environmental Research Paper Air Force Geophysics Lab., Hanscom AFB, MA. Optical Physics Div.*, P. Tsipouras and H. B. Garrett, eds. (Air Force Geophysics Lab., 1979).
23. T. Harmel and M. Chami, "Determination of sea surface wind speed using the polarimetric and multidirectional properties of satellite measurements in visible bands," Geophys. Res. Lett. **39**(19), L19611 (2012).
24. D. D. Ngoc, H. Loisel, L. Duforet-Gaurier, C. Jamet, V. Vantrepotte, C. Goyens, H. C. Xuan, N. N. Minh, and T. N. Van, "Atmospheric correction algorithm over coastal and inland waters based on the red and NIR bands: application to Landsat-8/OLI and VNREDSat-1/NAOMI observations," Opt. Express **27**(22), 31676–31697 (2019).
25. L. B. Liao, S. Weiss, S. Mills, and B. Hauss, "Suomi NPP VIIRS day-night band on-orbit performance," J. Geophys. Res.: Atmos. **118**(22), 12,705–12,718 (2013).
26. B. Han, H. Loisel, V. Vantrepotte, X. Mériaux, P. Bryère, S. Ouillon, D. Dessailly, Q. Xing, and J. Zhu, "Development of a Semi-Analytical Algorithm for the Retrieval of Suspended Particulate Matter from Remote Sensing over Clear to Very Turbid Waters," Remote Sens. **8**(3), 211–234 (2016).